Document downloaded from:

http://hdl.handle.net/10251/176418

This paper must be cited as:

Sánchez Tovar, R.; Blasco-Tamarit, E.; Fernández Domene, RM.; Villanueva-Pascual, M.; Garcia-Anton, J. (2020). Electrochemical formation of novel TiO2-ZnO hybrid nanostructures for photoelectrochemical water splitting applications. Surface and Coatings Technology. 388:1-11. https://doi.org/10.1016/j.surfcoat.2020.125605

The final publication is available at

https://doi.org/10.1016/j.surfcoat.2020.125605

Copyright Elsevier

Additional Information

Journal Pre-proof

Electrochemical formation of novel TiO2-ZnO hybrid nanostructures for photoelectrochemical water splitting applications

R. Sánchez-Tovar, E. Blasco-Tamarit, R.M. Fernández-Domene, M. Villanueva-Pascual, J. García-Antón

PII: S0257-8972(20)30274-7

DOI: https://doi.org/10.1016/j.surfcoat.2020.125605

Reference: SCT 125605

To appear in: *Surface & Coatings Technology*

Received date: 7 January 2020

Revised date: 6 March 2020

Accepted date: 8 March 2020

Please cite this article as: R. Sánchez-Tovar, E. Blasco-Tamarit, R.M. Fernández-Domene, et al., Electrochemical formation of novel TiO2-ZnO hybrid nanostructures for photoelectrochemical water splitting applications, *Surface & Coatings Technology* (2020), https://doi.org/10.1016/j.surfcoat.2020.125605

This is a PDF file of an article that has undergone enhancements after acceptance, such as the addition of a cover page and metadata, and formatting for readability, but it is not yet the definitive version of record. This version will undergo additional copyediting, typesetting and review before it is published in its final form, but we are providing this version to give early visibility of the article. Please note that, during the production process, errors may be discovered which could affect the content, and all legal disclaimers that apply to the journal pertain.

© 2020 Published by Elsevier.

Journal Pre-proof

Electrochemical formation of novel TiO_2-ZnO hybrid nanostructures for photoelectrochemical water splitting applications

R. Sánchez-Tovar[a,b], E. Blasco-Tamarit[a], R.M. Fernández-Domene[a], M. Villanueva-Pascual[a], J. García-Antón[a]*

[a] *Ingeniería Electroquímica y Corrosión (IEC), Instituto Universitario de Seguridad Industrial, Radiofísica y Medioambiental (ISIRYM), Universitat Politècnica de València, Camino de Vera s/n, 46022 Valencia, Spain.* * *jgarciaa@iqn.upv.es*

[b]*Departamento de Ingeniería Química, Universitat de València, Av de les Universitats, s/n, 46100 Burjassot, Spain*

Abstract

In this study, hybrid ZnO-TiO_2 nanostructures have been synthesised by means of a simple electrochemical anodisation of titanium and subsequently ZnO electrodeposition. The influence of $Zn(NO_3)_2$ concentration and temperature during the electrodeposition process was evaluated. Different techniques were used to analyse the synthesised nanostructures, notably Field Emission Scanning Electron Microscopy (FE-SEM) with Energy-dispersive X-ray spectroscopy (EDX) and Confocal Microscopy with Raman spectroscopy coupled with an Atomic Force Microscope. Photoelectrochemical water splitting tests were also performed at the hybrid nanostructures. According to the results, the photoelectrochemical response of the specimens increases with the addition of ZnO, besides the hybrid nanostructures obtained at 25 ºC and using a $Zn(NO_3)_2$ concentration of 1 mM showed photocurrent densities 80% higher than the ones obtained for TiO_2 nanotubes. Analysis of Variance of the data confirms the obtained results.

Keywords: hybrid nanostructures, titanium dioxide, zinc oxide, photoelectrochemical water splitting.

Journal Pre-proof

1. Introduction

Titanium dioxide (TiO_2) is one of the most studied materials in the photocatalysis field, due to its outstanding properties [1], such as high electron carriers movement, high mechanical and corrosion resistance, chemical stability, environmental friendly, high photocatalytic activity and relative low cost when compared with other materials used as photocatalysts. Due to these properties, it can be used in several energy and environmental applications, for instance, as photoelectrode in dye sensitised solar cells, in photoelectrochemical water splitting for hydrogen production or for the photo oxidation of recalcitrant organic pollutants [2-4]. For all these applications where TiO_2 acts as the photoanode of the process, the relative surface/area is crucial to obtain high efficiencies, being the reason for nanoscaling the TiO_2 in the form of nanotubes, nanosheets, nanowires, nanoflowers and so on [5]. Especially, TiO_2 nanotubes constitute a matrix with a very high surface/area ratio which also creates a pathway for the electrons that, in turn, could reduce the recombination between the electron and hole pairs [1]. Several techniques are used to form TiO_2 nanotubes, being the chemical methods, such as hydrothermal or sol-gel processes, the most investigated [6]. However, the electrochemical anodisation process, in particular, when it is performed under controlled hydrodynamic conditions (using an rotating disc electrode for the working electrode), is a relatively novel technique. This process permits the formation of ordered TiO_2 nanotubes which can be tailored by changing the anodisation parameters, such as potential, time, voltage, etc [7]. Despite of all the advantages shown for the TiO_2 nanotubes as photocatalyst, it is important to point out that the band gap of this material in the anatase phase, which is the most studied phase for TiO_2 in photocatalysis due to its high conductivity [8, 9], is roughly 3.2 eV, limiting its photocatalytic applications to UV irradiation. This is a very negative aspect, since it restricts the use of TiO_2 as

photocatalyst using solar radiation, if considered that more than 40% of the solar spectrum corresponds to visible light and only 5-8% is associated to UV one [10, 11].

In order to solve this drawback, several options are found in the literature, i.e. doping of TiO_2 with noble metals [12]. The inconvenience of this procedure is the cost of the nanoparticles (platinum, silver or gold among others). In this work, the formation of hybrid TiO_2-ZnO nanostructures is proposed as an alternative and low cost methodology for the decoration of TiO_2 with noble metals. ZnO is a promising semiconductor which could be used as photocatalyst, in particular, due to its flexibility in the fabrication process and obtained morphology [13, 14]. It has a wide band gap (3.4 eV), similar to the one presented for TiO_2 in anatase phase, however, the large excitation binding energy of ZnO (60 meV) makes it promising as photoanode in photoelectrochemical processes [15]. As for TiO_2, one of the main disadvantages of using ZnO as photocatalyst is its large band gap value. Besides, the quick recombination of the photogenerated electron-hole pairs limits the use of ZnO in photoelectrochemical applications [16-18]. Other than this, stability of ZnO under UV light in aqueous solutions is limited, which reduces more its photocatalytic applications.

In order to sort out the drawbacks presented by the TiO_2 and ZnO nanostructures individually, the combination of TiO_2 with ZnO in one nanostructure (hybrid TiO_2-ZnO nanostructures), is proposed in this work to solve these issues; i.e. with this heterojunction the electron-transfer properties of the two semiconductors are improved. In fact, the heterostructure of these two materials, with similar band gaps (3.2 and 3.4 eV, for anatase-TiO_2 and ZnO, respectively), will take advantage of the more negative balance between the value of the conduction band edge of ZnO and the TiO_2 and the electrons will be transferred from the conduction band of ZnO to the conduction band of

TiO_2. On the contrary, holes will be transferred from the valence band of TiO_2 to the valence band of ZnO. In this way, the high activity of TiO_2 together with the high electron mobility of ZnO, may reduce the electron-hole pairs recombination and, consequently, increase the efficiency of the process [19-21].

Furthermore, TiO_2 could provide a protective matrix to ZnO which might reduce the dissolution problems of ZnO under UV light irradiation.

Other authors have also synthesised TiO_2-ZnO nanostructures by hydrothermal methods [16]. The main problem of this methodology is the number of reactants involved (such as zinc acetate, sodium hydroxide, ethanol and ethylenediamine) and the high temperatures and time (160 ºC during 8 h) involved in the process. Several works synthesised the hybrid nanostructures in a two-step process: first the TiO_2 nanostructures are formed by electrochemical anodisation and then, a subsequent electrodeposition of ZnO is carried out. Electrodeposition is usually performed using zinc acetate [22, 23] or zinc nitrate electrolytes [19, 24-26] with addition of ethanol and/or temperatures of the order of 65 ºC or higher.

Nevertheless, we did not find in the literature any work which synthesised hybrid TiO_2-ZnO nanostructures by titanium anodisation under hydrodynamic conditions (it was demonstrated in a previous work that hydrodynamic conditions improved the photocatalytic response of the nanostructures [11]) and subsequent ZnO electrodeposition without heating and/or the addition of ethanol. Hence, the objective of this work is the formation of hybrid TiO_2-ZnO nanostructures by electrochemical anodisation of titanium at 3000 rpm and subsequent ZnO electrodeposition from different concentrations of $Zn(NO_3)_2$ (1 to 5 mM, similar to those values found in the literature [19, 24, 26]) at different temperatures (25 to 65 ºC). The structural properties

of the nanostructures will be characterised by several microscopy techniques: Field Emission Scanning Electronic Microscopy (FE-SEM) with Energy-dispersive X-ray spectroscopy (EDX), Confocal Raman Spectroscopy and Atomic Force Microscopy (AFM). Photoelectrochemical water splitting tests will be carried out in order to evaluate the suitability of the hybrid nanostructures as photocatalysts. All the results will be analysed statistically using the Analysis of Variance of the data.

2. Experimental procedure

2.1. Hybrid nanostructure formation

The hybrid nanostructures were formed in a two-step process, electrochemical anodisation of titanium, followed by the ZnO electrodeposition on the TiO_2. Prior to anodisation, the titanium rods (8 mm in diameter) were wet abraded with different SiC papers grades (from 220 to 4000), then the titanium specimen was sonicated for 2 min in an ethanol solution. Finally, the titanium rod was rinsed with water and dried with air. Electrochemical anodisation was carried out with the titanium rod as the anode and using a platinum foil as the cathode. A potential difference of 55 V between anode and cathode was applied during 30 min under hydrodynamic conditions (3000 rpm); a rotating disk electrode with control of rotation speed was used to stablish this condition [27]. The electrolyte for anodisation consisted of ethylene glycol based with concentrations of 0.05 M of NH_4F and 1M of H_2O.

Once the titanium was anodised, the TiO_2 formed nanostructures were put in a electrochemical cell and connected as a working electrode. An Ag/AgCl 3M KCl electrode was used as the reference and a platinum tip as the counter electrode. A

solution of $Zn(NO_3)_2 \cdot 6H_2O$ was employed for the ZnO electrodeposition, at three different concentrations, notably: 1, 3 and 5 mM. The potential applied for electrodeposition was $-0.8V_{Ag/AgCl}$ for 1 h and the temperature was set at 25, 45 and 65 ºC.

Once the hybrid nanostructure was produced, it was cut in a slice of approximately 0.5 cm, then, the specimens were introduced in a horizontal oven to transform the amorphous structure into a crystalline one. The annealing treatment was carried out for 1 h at 450 ºC, using a heating rate of 15 ºC/min.

2.2. Characterisation of the nanostructures

2.2.1. Structural Characterisation

The morphology of the hybrid nanostructures was characterised using a Field Emission Scanning Electron Microscope (FE-SEM). The microscope was equipped with an Energy-dispersive X-ray spectroscope (EDX) that was used to determine the presence of different elements in the nanostructures.

Additionally, the crystalline structure of the samples was analysed by Confocal Raman Microscopy. A blue laser (488 nm) was used for the characterisation.

An Atomic Force Microscope (AFM) was used to characterise the nano-scale roughness of the hybrid nanostructures. In this case, the Sa (arithmetical mean height of the surface) was the parameter calculated to evaluate the surface roughness of the samples. The AC mode (an intermittent contact regimen) was used with an oscillating cantilever (0.5 V).

Journal Pre-proof

2.2.2. Electrochemical Characterisation

Photoelectrochemical water splitting tests for hydrogen production were performed by using a solar simulator (AM 1.5, 100 $mW \cdot cm^{-2}$) connected to a potentiostat. During the experiments, the potential was sweeped from $-1V_{Ag/AgCl}$ until $0.8\ V_{Ag/AgCl}$ and light was intermittently chopped (20 mV without light and 60 mV with light). The hybrid nanostructures were used as the working electrode (an area of 0.26 cm^2 was exposed during the tests), an Ag/AgCl 3M KCl was the reference electrode and a platinum tip the counter electrode. The electrolyte used for the tests was 0.1M NaOH.

2.3. Statistical analysis

A surface response analysis was carried out with the software Statgraphics Centurion. The photocurrent density obtained at the end of the photoelectrochemical water splitting tests was used as the response variable, taking into account two experimental factors: the $Zn(NO_3)_2$ concentration and the temperature used during electrodeposition. Since each factor possesses 3 levels (1, 3 and 5 mM for $Zn(NO_3)_2$ and 25, 45 and 65 ºC for temperature) a factorial of 3 levels design: 3^2 was performed.

3. Results and discussion

3.1. Electrochemical hybrid nanostructure formation

The hybrid nanostructures were formed in a two-step process: first a titanium anodisation under hydrodynamic conditions was carried out and, then an electrochemical zinc oxide electrodeposition over the TiO_2 nanostructures was performed. Figure 1 shows the current densities obtained during the electrochemical anodisation process. In this figure three different stages can be observed (see zoom insert in Figure 1). The first one (stage I) is characterised by a decrease of the current

density with time, until reaching a minimum current density value. This stage is related with the formation of a TiO_2 layer over the titanium substrate, which is responsible of the resistance increase, and consequently of the current density decrease [1, 28-30]. Equations 1 to 3 summarise the reactions that occur during stage I.

$$Ti \rightarrow Ti^{4+} + 4e^- \quad (1)$$

$$Ti^{+4} + 2H_2O \rightarrow TiO_2 + 4H^+ \quad (2)$$

$$Ti + 2H_2O \rightarrow TiO_2 + 4H^+ + 4e^- \quad (3)$$

Then, once the minimum value is reached, the current density values increase until a maximum (stage II). At this stage, the TiF_6^{2-} complex is formed due to the reaction between fluorides and TiO_2 (see equation 4). This complex is the responsible for the initial pits on the TiO_2 layer, which generates an increase in the current densities [1, 30, 31].

$$TiO_2 + 4H^+ + 6F^- \rightarrow [TiF_6]^{2-} + 2H_2O \quad (4)$$

Finally, the stage III is characterised by the formation of the nanostructure consequence of an equilibrium between the formation and dissolution of TiO_2. Due to this competitive behaviour, current densities during the stage III remain almost constant with time [1, 7, 30].

Once the TiO_2 nanostructure is formed, ZnO was electrodeposited from a $Zn(NO_3)_2$ solution. The ZnO electrodeposition is based on the generation of OH^- ions on the TiO_2 surface by means of the reduction of precursors such as O_2, NO_3^- and H_2O_2 in an

aqueous solution containing zinc ions, according to the following reactions (equations 5 to 9) [15, 19, 26, 32].

$$Zn(NO_3)_2 \rightarrow Zn^{2+} + 2NO_3^- \quad (5)$$

$$NO_3^- + H_2O + 2e^- \rightarrow NO_2^- + 2OH^- \quad (6)$$

$$Zn^{2+} + 2OH^- \rightarrow Zn(OH)_2 \quad (7)$$

$$Zn(OH)_2 \rightarrow ZnO + H_2O \quad (8)$$

$$Zn^{2+} + NO_3^- + 2e^- \rightarrow ZnO + NO_2^- \quad (9)$$

The reduction of the nitrate to nitrite is catalysed by the Zn^{+2} ions (equation 6) and then, the latter are adsorbed on the TiO_2 surface liberating OH^- ions. Additionally, Zn^{+2} ions precipitate with the OH^- anions, and consequently, the $Zn(OH)_2$ is formed (equation 7). Zinc hydroxide spontaneously dehydrates and it is transformed into ZnO and H_2O (Equation 8). Equation 9 summarises all the electrodeposition process.

Figure 2 shows the current densities during ZnO electrodeposition on TiO_2 during time for the different $Zn(NO_3)_2$ concentrations (1, 3 and 5 mM) and temperatures (25, 45 and 65 ºC) used during the process.

As it can be observed in Figure 2, the general trend for the current densities in the electrodeposition is the same regardless the initial $Zn(NO_3)_2$ concentration or the temperature during the process; i.e. during the first seconds of the process, the current density reaches its maximum value, which is related to the nucleation of the ZnO cristals [15], which means that OH^- formation takes place on the TiO_2 surface due to the reduction of nitrates, which makes possible the reaction of these ions with Zn^{+2}, and hence, the formation of ZnO. The higher values of current density for the nanostructures

obtained working at 65 ºC, may be related to a higher amount of ZnO crystals on TiO_2 [15, 26].

3.2. Morphology and composition of the hybrid nanostructures by FE-SEM–EDX analysis

In order to determine the morphology of the hybrid nanostructures FE-SEM images have been obtained. Figure 3 shows FE-SEM images of the hybrid nanostructures obtained from an 1mM $Zn(NO_3)_2$ solutions at different temperatures. Additionally, Figure 3 includes a FE-SEM image of a TiO_2 sample obtained by electrochemical anodisation where electrodeposition of ZnO has not been carried out (Figure 3a).

Figure 3a shows the top view of the TiO_2 nanostructure anodised at 3000 rpm where it is clearly observed an initiation layer that partially covers the entrance of the tubes. This initiation layer is typical of nanostructures synthesised in organic based electrodes [33, 34]. Figure 3a also shows that the initiation layer is removed or somehow detached in some parts of the surface due to the dynamic conditions during anodisation [11, 31]. The average diameter of the initiation layer pores is 100±10 nm. Figures 3b to 3d show the top view images of the hybrid nanostructures obtained by anodisation of titanium at 3000 rpm plus electrodeposition of ZnO from 1mM of $Zn(NO_3)_2$ at 25, 45 and 65 ºC, respectively. Two effects could be elucidated from the ZnO electrodeposition: first, the average diameter of the pores of the initiation layer is reduced, notably 80±10 nm at 25ºC, and 60±10 nm at 45 and 65 ºC (similar values were obtained when the $Zn(NO_3)_2$ concentration was increased at different temperatures). This fact might be related to a ZnO layer formed on the nanostructure that partially covers the surface. Regarding the second effect, some particles appear on the TiO_2 surface covering part of it. These

particles are bigger and become more geometrically defined with the increase of the temperature. Figure 3c shows that at 45 ºC the particles have a round shape with a very porous consistence; however, at 65 ºC (Figure 3d) the particles are more homogeneous with a plain, regular and compact shape. These particles may be related to ZnO crystals. Besides, if $Zn(NO_3)_2$ concentration increases and the electrodeposition takes place at 45 ºC or higher temperatures, the number of particles considerably increases (see for instance Figure 4, where FE-SEM images of hybrid TiO_2-ZnO nanostructures electrodeposited at 45 ºC and from 1 and 5 mM $Zn(NO_3)_2$ are shown). This effect could be negative, since all these particles are covering and partially blocking the entrances of the tubes and, consequently, decreasing the absorption of light. In fact, other authors which performed ZnO electrodeposition at high temperatures (80 ºC or above), also found that the ZnO crystals spilled over the TiO_2 nanotubes growing in an epitaxial form [19, 35, 36]. At 25 ºC, the number of ZnO crystals electrodeposited on TiO_2 surface is low, regardless the $Zn(NO_3)_2$ concentration (Figure 3b). Moreover, Figure 4a shows a backscattered electron FE-SEM image where it is clearly shown the presence of two different compounds in the hybrid nanostructures. One of those partially covers the tops of the nanotubes and forms the deposited particles. Figure 5 shows, as an example, a FE-SEM image of a cross section of a TiO_2 anodised nanostructure (Figure 5a), together with an image of the hybrid nanostructure obtained from 5mM of $Zn(NO_3)_2$ at 65 ºC (Figure 5b). Additionally, Figure 5 also shows that the nanotubular shape is maintained after ZnO electrodeposition, having the nanotubes a length of 5 ± 1 μm.

In order to check the composition of the hybrid nanostructures and to confirm the presence of Zn, EDX analysis was carried out. Figure 6 shows an example of EDX spectra of two hybrid nanostructures obtained from 1 mM $Zn(NO_3)_2$ at 25 ºC and from 5 mM $Zn(NO_3)_2$ at 65 ºC (Figures 6a and 6b, respectively). Figure 6 confirms that hybrid

nanostructures are composed by oxygen, titanium and zinc. In particular, EDX reveals that the average weight percent on the surface of the different elements is: O ~ 35-45 wt. %, Ti ~ 55-60 wt. % and Zn ~ 2-3 wt (Figure 6a). %. These values are in agreement with the ones found in literature [25]. This result is in agreement with the presence of two phases in Figure 4 and the electrodeposition of ZnO on TiO_2 nanotubes. Additionally, the composition of each element on the particles that cover the surface is: O ~ 40-50 wt. %, Ti ~ 25-35 wt. % and Zn ~ 30-40 wt. %, which confirms the increase of Zn content in the electrodeposited particles (Figure 6b).

3.3. Laser Confocal Microscopy with Raman spectroscopy evaluation

Once the presence of oxygen, titanium and zinc was demonstrated, Laser Confocal Microscopy with Raman spectroscopy was used in order to determine the different chemical bonds between these elements and, to evaluate the crystalline structure of the samples after the annealing treatment.

Figure 7 shows, as an example, the Raman spectra of a TiO_2 nanostructure anodised at 3000 rpm (without ZnO electrodeposited particles) and of three hybrid nanostructures obtained from 1, 3 and 5 mM $Zn(NO_3)_2$ at 65 ºC, respectively.

In Figure 7a two distinct parts can be observed, one at Raman shifts lower than 900 cm^{-1}, and the other at values between 1800 and 5400 cm^{-1}. It is remarkable that for the TiO_2 nanostructure, only the peaks associated to the Raman shifts lower than 900 cm^{-1} are present. The peaks which appear between 0 and 900 cm^{-1}; in particular at ~142, ~396, ~516 and ~639 cm^{-1} [16, 30, 37, 38] are related to the TiO_2 anatase phase. All the peaks associated to TiO_2 anatase phase are present in all the Raman spectra and have similar values and shape. Contrary to this, Figure 7a also shows, for the hybrid

nanostructures a pronounced peak with a maximum at ~4000 cm^{-1}, which may be associated with ZnO photoluminescence. Other authors [16, 39-41] also observed the photoluminescence phenomena of ZnO and they attributed this effect to band defects, such as oxygen vacancies or surface defects. Figure 7a shows that the band related to photoluminescence of ZnO increases when $Zn(NO_3)_2$ concentration also increases, which is in concordance with a higher amount of ZnO for the samples electrodeposited at higher $Zn(NO_3)_2$ concentrations. Photoluminiscence phenomena could be explained taking into consideration that during the ZnO electrodeposition, substitution of Ti^{+3} by the Zn^{+2} in Ti_2O_3 takes place, and, as a consequence of this, a great number of oxygen vacancies are created. Oxygen vacancies are the responsible for the creation of an excitation energy level near the bottom of the conduction band of the Ti_2O_3 lattice, where electrons can easily access [42]. Additionally, Figure 7b shows a magnification of the Raman spectra at low Raman shifts (300 to 800 cm^{-1}). In this figure a peak at roughly 438.5 cm^{-1} (indicated with a circle in the graph) could be elucidated for the hybrid nanostructures, which is more noticeable for nanostructures with more zinc content. This peak is attributed to the E2 mode of wurtzite hexagonal ZnO [16, 43, 44].

It is important to point out that the same peaks were obtained for all the hybrid nanostructures, showing the same tendency for the different $Zn(NO_3)_2$ concentrations. There is not a clear trend of the Raman spectra obtained from the nanostructures with the temperature of the process.

3.4. Atomic Force Microscopy

Figure 8 shows, as an example, the AFM 2D and 3D images of the TiO_2 nanotubes (Sa = 49.41 nm) and two hybrid nanostructures obtained from 5 mM $Zn(NO_3)_2$ at 25 and 65

ºC (Sa values of 96.87 and 112.44 nm, respectively). The Sa values for the hybrid nanostructures were higher than those obtained for the TiO_2 nanotubes. In particular, as shown in Figure 8, Sa values obtained for hybrid nanostructures increase when the electrodeposition temperature rises. Besides, Sa values are higher for the hybrid nanostructures electrodeposited at higher $Zn(NO_3)_2$ concentrations, for instance, when electrodeposition was carried out at 25 ºC, the Sa values were 63.06, 71.12 and 96.87 nm at 1, 3 and 5 mM of $Zn(NO_3)_2$, respectively. High values of roughness might be beneficial in order to increase the surface area for photocatalytic applications. However, if the roughness increase is related to particles electrodeposited over the nanotubes (i.e. blocking the mouth of the nanotubes and, consequently, hindering light absorption), the effect may be detrimental.

3.4. Photoelectrochemical water splitting tests

Figure 9 shows the photoelectrochemical water splitting tests for the hybrid nanostructures at the different $Zn(NO_3)_2$ concentrations and temperatures during electrodeposition. In Figure 9 it can be observed that, in general, the best photoelectrochemical response is associated with the specimens obtained at lower temperatures and lower initial concentration of $Zn(NO_3)_2$, showing the highest photocurrents the specimens obtained from a 1 mM $Zn(NO_3)_2$ concentration and at 25 ºC. Two negative effects observed at higher $Zn(NO_3)_2$ concentrations and electrodeposition temperatures may explain this behaviour. On the one hand, the pores of the initiation layer become smaller and the partially detached areas are covered with ZnO. On the other hand, the amount of ZnO crystals is higher and the crystals are

bigger. These two effects diminish the absorption of light of the hybrid nanostructures and in turns decrease the photoelectrochemical response for water splitting.

Figure 9 also shows that, in general, the photocurrents does not vary applying voltages higher than -0.6 $V_{Ag/AgCl}$, which is an advantage, since lower polarizations need to be applied for the photoelectrochemical process. Additionally, lower potential values could be obtained from renewable sources [45]. Attending to the dark currents, they are really low in all the cases (even when 0.8 $V_{Ag/AgCl}$ are applied), which denotes the stability of the samples (there is no electrochemical oxidation) and their suitability for photoelectrochemical water splitting applications.

The photoelectrochemical water splitting response of a TiO_2 nanostructure was included in Figure 9 in order to compare the results with those obtained for the hybrid nanostructures. As it can be denoted from Figure 9, in general, the photocurrents obtained for all the hybrid nanostructures are higher than the ones achieved for the TiO_2 nanotubes. Especially, the photocurrents obtained for the hybrid nanostructure electrodeposited at 25 ºC and using 1 mM of $Zn(NO_3)_2$ are 82% higher than the corresponding to the TiO_2 nanotubes. Additionally, the higher separate efficiency of photogenerated charges in the hybrid nanostructures, can be denoted by the photocurrent response of the hybrid samples at lower potential values (see Figure 9) [19]. These results are promising since this is the first time, to the best of our knowledge, that an hybrid TiO_2-ZnO nanostructure is fabricated by titanium anodisation under hydrodynamic conditions and subsequently $Zn(NO_3)_2$ electrodeposition at roughly room temperature and without additional chemicals, such as ethanol [24, 26]. Taking into account the good results, future works should be focused on the formation of hybrid nanostructures from lower $Zn(NO_3)_2$ concentrations and at 25 ºC.

3.5. Statistical analysis

Table 1 shows the analysis of the Variance for the photocurrent density obtained from the statistical design. Only the temperature effect results statistically significant for photoelectrochemical water splitting, since its p-value is lower than 0.05 (p-value = 0.0134). That means that, if the temperature during the electrodeposition of ZnO is low (along the studied range), the formed hybrid nanostructures possess higher photocurrent densities for photoelectrochemical water splitting applications. However, the quadratic effects of temperature and $Zn(NO_3)_2$ concentration have p-values considerably higher than 0.05 (0.7851 and 0.4709, respectively), therefore, they were excluded from the analysis. It is noticeable that the simple effect of $Zn(NO_3)_2$ concentration was not excluded from the analysis, since the interaction between $Zn(NO_3)_2$ and temperature has a p-value of 0.0577. The new analysis (excluding the quadratic effects of temperature and $Zn(NO_3)_2$ concentration) is shown in Table 2. Table 2 indicates that both temperature and the interaction between temperature and $Zn(NO_3)_2$ concentration result statistically significant (p-values of 0.0083 and 0.0432, respectively). As it can be concluded from the interaction plot (Figure 10), in order to synthesise the most suitable hybrid nanostructures (i.e. to obtain high photocurrent density values), it is not only important to perform the electrodeposition of ZnO at 25 ºC, but also to use low $Zn(NO_3)_2$ concentrations (1mM).

4. Conclusions

In this work, hybrid TiO_2-ZnO nanostructures have been synthesised by electrochemical anodisation of titanium under hydrodynamic conditions and subsequent ZnO electrodeposition from $Zn(NO_3)_2$ at different concentrations (1, 3 and 5 mM) and

temperatures (25, 45 and 65 ºC). FE-SEM images revealed a nanotubular structure for the hybrid samples. Besides, this technique also showed that the ZnO electrodeposited homogeneously throughout the surface. Moreover, at higher temperatures and $Zn(NO_3)_2$ concentrations, ZnO crystals precipitated on the TiO_2. Additionally, the size and the number of crystals increased with both temperature and $Zn(NO_3)_2$ concentration. Confocal Raman Microscopy and EDX analysis showed that the samples contain oxygen, titanium and zinc in the form of anatase TiO_2 and hexagonal wurtzite ZnO. AFM evaluation indicated that the roughness of the hybrid nanostructures increased in comparison to the one obtained for the TiO_2 nanotubes. Additionally, the roughness was higher for the nanostructures obtained at greater $Zn(NO_3)_2$ concentrations and electrodeposition temperatures.

The photoelectrochemical water splitting tests showed that the hybrid nanostructures with higher photocurrent densities are the ones synthesised at lower $Zn(NO_3)_2$ concentrations and temperatures, with higher photoelectrochemical response in comparison to a TiO_2 nanostructure anodised at the same conditions but without ZnO.

The statistical analysis concluded that temperature and the interaction between temperature and $Zn(NO_3)_2$ concentration are statistically significant parameters on photocurrent densities.

To sum up, in this study it has been demonstrated the suitability of hybrid TiO_2-ZnO nanostructures obtained by electrochemical anodisation of titanium under hydrodynamic conditions and subsequent electrodeposition of ZnO from 1 mM $Zn(NO_3)_2$ and at 25 ºC. This process shows an important advantage with respect to the

literature, since lower temperatures allow the formation of hybrid nanostructures without the addition of chemicals, such as ethanol.

Acknowledgements: Authors thank for the financial support to the Ministerio de Economía y Competitividad (Project Code: CTQ2016-79203-R), for its help in the Laser Raman Microscope acquisition (UPOV08-3E-012) and for the co-finance by the European Social Fund. Authors also thank the Generalitat Valenciana for its financial support through the project: IDIFEDER/018/044 co-finance by the European Social Fund. Authors also thank to the UPV for the concession of a post-doctoral grant (PAID-10-17) to Ramón M. Fernández Domene.

References

[1] P. Roy, S. Berger, P. Schmuki, TiO_2 nanotubes: synthesis and applications, Angew. Chem. Int. Ed., 50 (2011) 2904-2939.

[2] J.M. Macak, H. Tsuchiya, A. Ghicov, K. Yasuda, R. Hahn, S. Bauer, P. Schmuki, TiO_2 nanotubes: self-organized electrochemical formation, properties and applications, Curr. Opin. Solid St. Mater. Sci., 11 (2007) 3-18.

[3] A. Ghicov, P. Schmuki, Self-ordering electrochemistry: a review on growth and functionality of TiO_2 nanotubes and other self-aligned MO_x structures, Chem. Commun., 2009, 2791–2808.

[4] I. Paramasivam, H. Jha, N. Liu, P. Schmuki, A review of photocatalysis using self-organized TiO_2 nanotubes and other ordered oxide nanostructures, Small, (2012) 20, 3073–3103.

Journal Pre-proof

[5] Xuemei Zhou, Nhat Truong Nguyen, Selda Özkan, Patrik Schmuki, Anodic TiO_2 nanotube layers: Why does self-organized growth occur—A mini review, Electrochem. Commun. 46 (2014) 157–162.

[6] P. Qiu, X. Sun, Y. Lai, P. Gao, C. Chen, L. Ge, N-doped TiO_2@TiO_2 visible light active film with stable and efficient photocathodic protection performance, Journal of Electroanalytical Chemistry 844 (2019) 91-98.

[7] R. Sánchez-Tovar, K. Lee, J. García-Antón, P. Schmuki, Formation of anodic TiO_2 nanotube or nanosponge morphology determined by the electrolyte hydrodynamic conditions, Electrochem. Commun. 26 (2013) 1-4.

[8] D. Regonini, A. Jaroenworaluck, R. Stevens, C.R. Bowen, Effect of heat treatment on the properties and structure of TiO_2 nanotubes: phase composition and chemical composition, Surf. Interface Anal., 42 (2010) 139-144.

[9] R.M. Fernández-Domene, R. Sánchez-Tovar, S. Sánchez-González, J. García-Antón, Photoelectrochemical characterization of anatase-rutile mixed TiO2 nanosponges, Int. J. Hydrogen Energy, 41 (2016) 18380-18388.

[10] L.-k. Tsui, M. Saito, T. Hommab, G. Zangari, Trap-state passivation of titania nanotubes by electrochemical doping for enhanced photoelectrochemical performance, J. Mater. Chem. A, 3 (2015) 360-367.

[11] J. Borràs-Ferrís, R. Sánchez-Tovar, E. Blasco-Tamarit, R.M. Fernández-Domene, J. García-Antón, Effect of Reynolds number and lithium cation insertion on titanium anodization, Electrochim. Acta 196 (2016) 24-32.

[12] A. John, J. Naduvath, S. Remillard, S. Shaji, P.A. De Young, Z. T. Kellner, S. Mallick, M. Thankamoniamma, G. S. Okram, R. Reen, P., A simple method to fabricate metal doped TiO_2 nanotubes, Chemical Physics 523 (2019) 198-204.

[13] H. Guan, W. Xu, Xue Li, Hui Peng, Yi Feng, Jian Zhang, Chuannan Li, Implementation of photothermal annealing on ZnO electron transporting layer for high performance inverted polymer solar cells, Mater. Letter 163 (2016) 69-71.

[14] J. Deng, M. Wang, J. Liu, X. Song, Z. Yang, Arrays of ZnO/AZO (Al-doped ZnO) nanocables: A higher open circuit voltage and remarkable improvement of efficiency for CdS-sensitized solar cells, J. Colloid Interface Sci 418 (2014) 277-282.

[15] S. Dai, Y. Li, Z. Du, K. R. Carter, Electrochemical Deposition of ZnO Hierarchical Nanostructures from Hydrogel Coated Electrodes, J. of electrochem Soc. 160 (2013) D156-D162.

[16] L. Lin, Y. Yang, L. Men, X. Wang, D. He, Y. Chai, B. Zhao, S. Ghoshroy, Q. Tang, A highly efficient TiO_2@ZnO n–p–n heterojunction nanorod photocatalyst, Nanoscale 5 (2013) 588-593.

[17] S. Hernández, D. Hidalgo, A. Sacco, A. Chiodoni, A. Lamberti, V. Cauda, E. Tresso, G. Saracco, Comparison of photocatalytic and transport properties of TiO_2 and ZnO nanostructures for solar-driven water splitting, Phys. Chem. Chem. Phys. 17 (2015) 7775-7786.

[18] X. Chen, S. S. Mao, Titanium Dioxide Nanomaterials: Synthesis, Properties, Modifications, and Applications, Chem. Rev. 107 (2007) 2891-2959.

[19] Z. Zhang, Y. Yuan, L. Liang, Y. Cheng, G. Shi, L. Jin, Preparation and photoelectrocatalytic activity of ZnO nanorods embedded in highly ordered TiO_2 nanotube arrays electrode for azo dye degradation, J. Hazard. Mater 158 (2008) 517-522.

[20] F.-X. Xiao, B. Liu, In situ etching-induced self-assembly of metal cluster decorated one-dimensional semiconductors for solar-powered water splitting: unraveling

cooperative synergy by photoelectrochemical investigations, Nanoscale 9 (2017) 17118-17132.

[21] L. Zhang, H. B. Wu, B. Liu, X. Wen, Formation of porous SnO_2 microboxes via selective leaching for highly reversible lithium storage, Energ. Environmen. Sci. 7 (2014) 1013-1017.

[22] Y. Liao, K. Zhang, X. Wang, D. Zhang, Y. Li, H. Su, H. Zhang, Z. Zhong, Preparation of ZnO@TiO_2 nanotubes heterostructured film by thermal decomposition and their photocatalytic performances, RSC advances 8 (2018) 8064-8070.

[23] G.Z. Li, Q.M. Zhao, H.L. Yang, Z.T. Liu, Fabrication and characterization of ZnO-coated TiO_2 nanotube arrays, Compos. Interfaces 23 (2016) 125-132.

[24] S. Yao, X. Feng, J. Lu, Y. Zheng, X. Wang, A.A. Volinsky, L.-N. Wang, Antibacterial activity and inflammation inhibition of ZnO nanoparticles embedded TiO_2 nanotubes, Nanotechnology 29 (2018) 244003-244013.

[25] W. Liu, P. Su, S. Chen, N. Wang, Y. Ma, Y. Liu, J. Wang, Z. Zhang, H. Li, T.J. Webster, Synthesis of TiO_2 nanotubes with ZnO nanoparticles to achieve antibacterial properties and stem cell compatibility, Nanoscale 6 (2014) 9050-9062.

[26] S.W. NG, F.K. Yam, Z. Hassan, Rapid formation of zinc oxide nanosheets on titanium dioxide nanotubes through electrochemical method, Optoelectron. Adv. Mater.-Rapid Commun. 9 (2015) 1429-1434.

[27] B. Lucas-Granados, R. Sánchez-Tovar, R. M. Fernández-Domene, J. García-Antón, Controlled hydrodynamic conditions on the formation of iron oxide nanostructures synthesized by electrochemical anodization: Effect of the electrode rotation speed, Appl. Surf. Sci. 392 (2017) 503-513.

[28] T.T. Isimjan, S. Rohani, A.K. Ray, Photoelectrochemical water splitting for hydrogen generation on highly ordered TiO_2 nanotubes fabricated by using Ti as cathode, Int. J. Hydrogen Energy 37 (2012) 103–108.

[29] D. Regonini, C.R. Bowen, A. Jaroenworaluck, R. Stevens, A review of growth mechanism, structure and crystallinity of anodized TiO_2 nanotubes, Mater. Sci. Eng., R 74 (2013) 377–406.

[30] R. Sánchez-Tovar, E. Blasco-Tamarit, R. M. Fernández-Domene, B. Lucas-Granados, J. García-Antón, Should TiO_2 nanostructures doped with Li+ be used as photoanodes for photoelectrochemical water splitting applications? J. Catal. 349 (2017) 41-52.

[31] R. Sánchez-Tovar, I. Paramasivam, K. Lee, P. Schmuki, Influence of hydrodynamic conditions on growth and geometry of anodic TiO_2 nanotubes and their use towards optimized DSSCs, J. Mater. Chem. 22 (2012) 12792–12795.

[32] G. H. A. Therese, P. V. Kamath, Electrochemical Synthesis of Metal Oxides and Hydroxides, Chem. Mater. 12 (2000) 1195-1204.

[33] S. Mohajernia, A. Mazare, E. Gongadze, V. Kralj-Iglič, A. Iglič, P. Schmuki, Self-organized, free-standing TiO2 nanotube membranes: Effect of surface electrokinetic properties on flow-through membranes, Electrochim. Acta 245 (2017) 25-31.

[34] P. Roy, S.P. Albu, P. Schmuki, TiO_2 nanotubes in dye-sensitized solar cells: Higher efficiencies by well-defined tube tops, Electrochem. Commun. 12 (2010) 949-951.

[35] S. Benkara, S. Zerkout, Preparation and characterization of ZnO nanorods grown into aligned TiO2 nanotube array, J. Mater. Environ. Sci. 1 (2010) 173-188.

[36] K. Yu, Z. Jin, X. Liu, J. Zhao, J. Feng, Shape alterations of ZnO nanocrystal arrays fabricated from $NH_3 \cdot H_2O$ solutions, Appl. Surf. Sci. 253 (2007) 4072-4078.

[37] H.-W. Cho, K.-L Liao, J.-S. Yang, J.-J Wu, Revelation of rutile phase by Raman scattering for enhanced photoelectrochemical performance of hydrothermally-grown anatase TiO_2 film, Appl. Surf. Sci. 440 (2018) 125-132.

[38] Z. Wei, C. Hsu, H. Almakrami, G. Lina, J. Hu, X. Jin, E. Agar, F. Liu, Ultra-high-aspect-ratio vertically aligned 2D MoS_2-1D TiO_2 nanobelt heterostructured forests for enhanced photoelectrochemical performance, Electrochim. Acta 316 (2019) 173-180.

[39] A. Kushwaha, M. Aslam, ZnS shielded ZnO nanowire photoanodes for efficient water splitting, Electrochim. Acta 130 (2014) 222–231.

[40] A. Kushwaha, H. Tyagi, M. Aslam, Role of defect states in magnetic and electrical properties of ZnO nanowires, AIP Adv. 3 (2013) 042110–042115.

[41] Y. Zhang, L. Wu, Y. Liu, E. Xie, Improvements to the hierarchically structured ZnO nanosphere based dye-sensitized solar cells, J. Phys. D: Appl. Phys. 42 (2009) 085105–085110.

[42] J. Liqiang, S. Xiaojun, X. Baifu, W. Baiqi, C. Weimin, F. Honggang, The preparation and characterization of La doped TiO2 nanoparticles and their photocatalytic activity, J. Solid State Chem. 177 (2004) 3375-3382.

[43] R. Zhang, P.-G. Yin, N. Wang, L. Guo, Photoluminescence and Raman scattering of ZnO nanorods, Solid State Sci. 11 (2009) 865-869.

[44] S. He, M. Zheng, L. Yao, X. Yuan, M. Li, L. Ma, W. Shen, Preparation and properties of ZnO nanostructures by electrochemical anodization method, Appl. Surf. Sci., 256 (2010) 2557-2562.

[45] L.J. Minggu, W.R.W. Daud, M.B. Kassim, An overview of photocells and photoreactors for photoelectrochemical water splitting, Int. J. Hydrogen Energy 35 (2010) 5233-5244.

Figure captions

Figure 1. Current densities vs time during anodisation of titanium at 55V for 30 min in ethlylene glycol based electrolyte with 0.1 M NH_4F and 1M H_2O stirring the electrode at 3000 rpm.

Figure 2. a) Current densities vs time during electrodeposition of $Zn(NO_3)_2$ 1 mM at 25, 45 and 65ºC. b) Current densities vs time during electrodeposition of $Zn(NO_3)_2$ 3 mM at 25, 45 and 65ºC, c) Current densities vs time during electrodeposition of $Zn(NO_3)_2$ 5 mM at 25, 45 and 65ºC.

Figure 3. FE-SEM images of: a TiO_2 nanostructure anodised at 3000 rpm (a), an hybrid nanostructure electrodeposited from $Zn(NO_3)_2$ 1 mM at 25 ºC (b), an hybrid nanostructure electrodeposited from $Zn(NO_3)_2$ 1 mM at 45 ºC (c) and an hybrid nanostructure electrodeposited from $Zn(NO_3)_2$ 1 mM at 65 ºC (d).

Figure 4. FE-SEM images of an hybrid nanostructure electrodeposited from $Zn(NO_3)_2$ 1 mM at 45 ºC (backscattered electron image) (a) and an hybrid nanostructure electrodeposited from $Zn(NO_3)_2$ 5 mM at 45 ºC (b).

Figure 5. Cross section of a TiO_2 nanostructure anodised at 3000 rpm (a) and of an hybrid nanostructure electrodeposited from $Zn(NO_3)_2$ 5 mM at 65 ºC (b).

Figure 6. EDX spectra of an hybrid nanostructure electrodeposited from $Zn(NO_3)_2$ 1 mM at 25 ºC with wt.%: O = 35.7; Ti = 61.3; Zn = 3.1 (a) and an hybrid nanostructure electrodeposited from $Zn(NO_3)_2$ 5 mM at 65 ºC with wt.%: O = 40.3; Ti = 28.4; Zn = 31.3 (b).

Figure 7. Raman spectra of a TiO_2 nanostructure anodised at 3000 rpm and of the hybrid nanostructures electrodeposited from $Zn(NO_3)_2$ at 1, 3 and 5 mM at 65 ºC.

Figure 8. Atomic Force Microscope 2D and 3D images of the nanostructures: a) TiO_2 nanostructure, b) hybrid ZnO-TiO_2 nanostructure synthesised at 5 mM ($Zn(NO_3)_2$ and at 25 ºC and c) hybrid ZnO-TiO_2 nanostructure synthesised at 5 mM ($Zn(NO_3)_2$ and at 65 ºC.

Figure 9. Current density vs. applied potential curves under dark and illumination conditions (AM 1.5) for the TiO_2 nanostructures together with the different hybrid nanostructures electrodeposited from $Zn(NO_3)_2$ 1 mM at 25, 45 and 65ºC a) $Zn(NO_3)_2$ 3 mM at 25, 45 and 65ºC b) and $Zn(NO_3)_2$ 5 mM at 25, 45 and 65ºC c).

Figure 10. Interaction between $Zn(NO_3)_2$ concentration and temperature of electrodeposition on photocurrent densities.

Journal Pre-proof

Table captions

Table 1. Analysis of variance for the photocurrent density taking into account the factors $Zn(NO_3)_2$ concentration, temperature of electrodeposition and the quadratic individual effects and between factors.

Table 2. Analysis of variance for the photocurrent density taking into account the factors $Zn(NO_3)_2$ concentration, temperature of electrodeposition and their interactions.

Journal Pre-proof

Table 1

	Sum of Squares	**Gl**	**Mean Square**	F_{ratio}	***p*-value**
$Zn(NO_3)_2$	0.0000016875	1	0.0000016875	0.13	0.7278
T	0.000114701	1	0.000114701	8.67	**0.0134**
$Zn(NO_3)_2^2$	0.00000738028	1	0.00000738028	0.56	0.4709
$Zn(NO_3)_2 \cdot T$	0.000059405	1	0.000059405	4.49	0.0577
T^2	0.00000103361	1	0.00000103361	0.08	0.7851
Residual error	0.000145575	11	0.0000132341		
Total	0.000599676	17			

Journal Pre-proof

Table 2

	Sum of Squares	Gl	Mean Square	F_{ratio}	*p*-value
$Zn(NO_3)_2$	0.0000016875	1	0.0000016875	0.14	0.7119
T	0.000114701	1	0.000114701	9.68	**0.0083**
$Zn(NO_3)_2$·T	0.000059405	1	0.000059405	5.02	**0.0432**
Residual error	0.000153989	13	0.0000118453		
Total	0.000599676	17			

Journal Pre-proof

Credit Author Statement

R. Sánchez-Tovar: Data supervision, writing, review and editing**.**

E. Blasco-Tamarit: Writing - review and editing.

R.M. Fernández-Domene, Methodology **and supervision.**

M. Villanueva-Pascual: Data acquisition, Writing - original draft.

J. García-Antón: Writing - review and editing.

Journal Pre-proof

Declaration of interests

☒ The authors declare that they have no known competing financial interests or personal relationships that could have appeared to influence the work reported in this paper.

☐The authors declare the following financial interests/personal relationships which may be considered as potential competing interests:

Journal Pre-proof

Highlights

TiO_2-ZnO nanostructures were obtained by anodization of Ti and ZnO electrodeposition

Electrodeposition was performed with different temperatures and amounts of $Zn(NO_3)_2$

Higher photocurrents are obtained with lower $Zn(NO_3)_2$ concentrations and temperatures

Temperature and interaction between it and $Zn(NO_3)_2$ are statistically significant

Journal Pre-proof

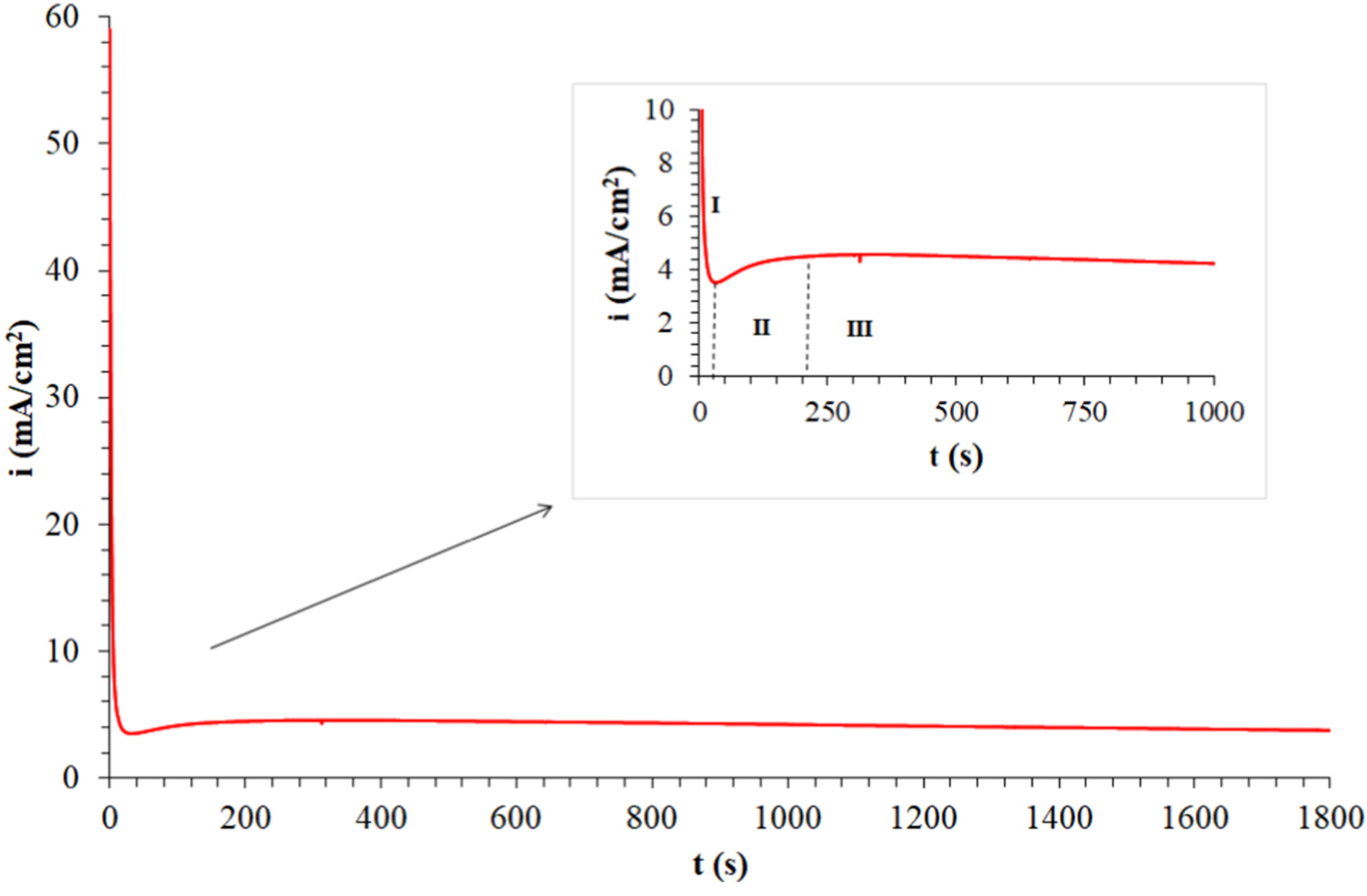
i (mA/cm²)
t (s)
0
10
20
30
40
50
60
0
200
400
600
800
1000
1200
1400
1600
1800
i (mA/cm²)
t (s)
I
II
III
0
2
4
6
8
10
0
250
500
750
1000

Figure 1

a) 1 mM $Zn(NO_3)_2$

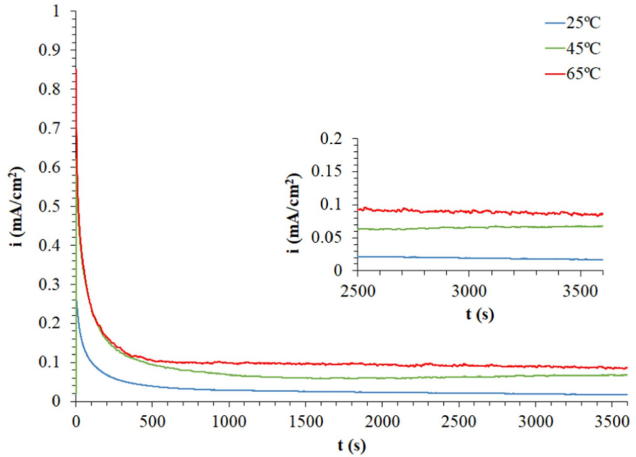

b) 3 mM $Zn(NO_3)_2$

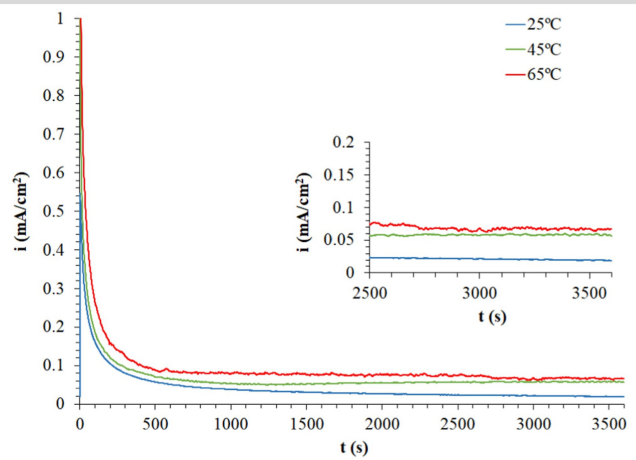

c) 5 mM $Zn(NO_3)_2$

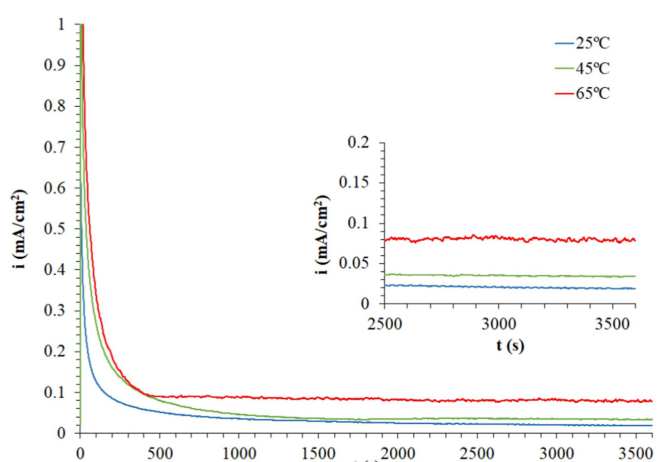

Figure 2

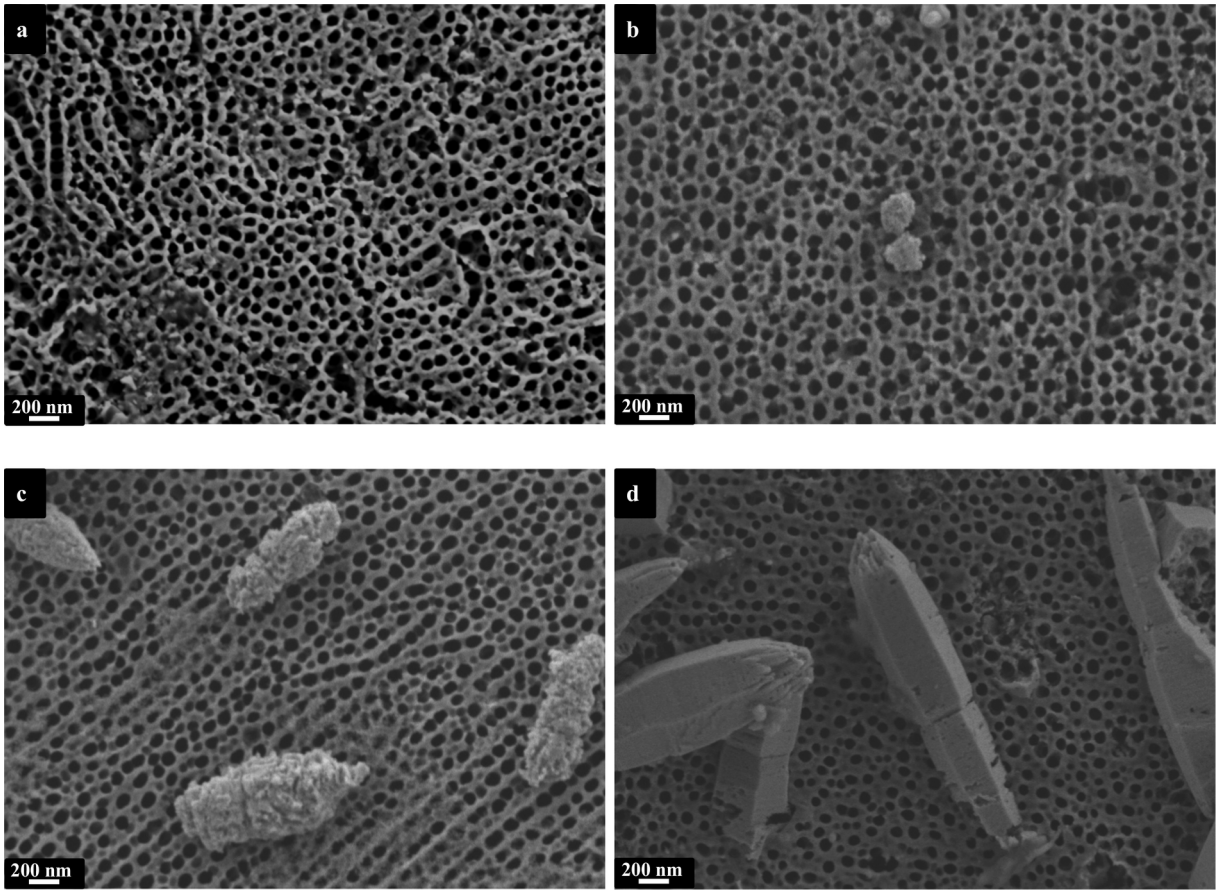

Figure 3

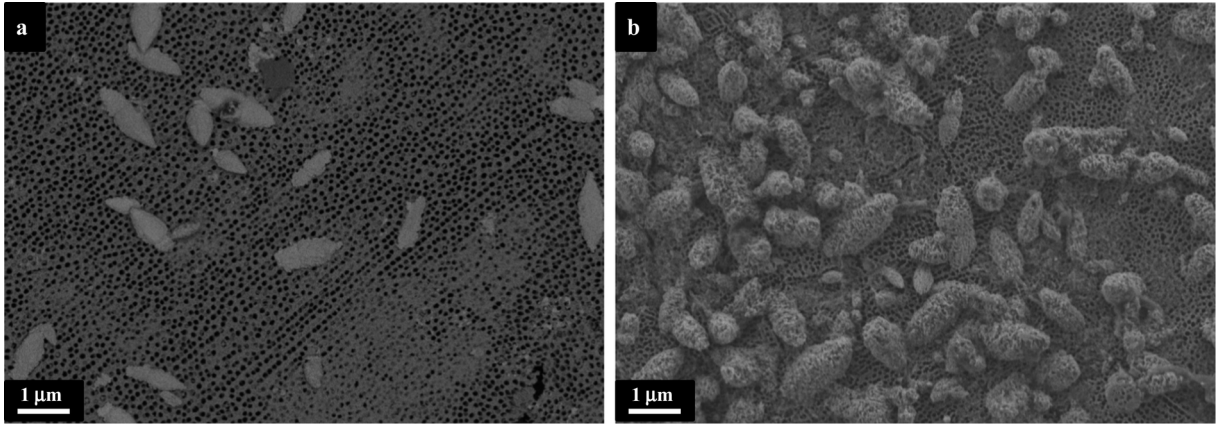

Figure 4

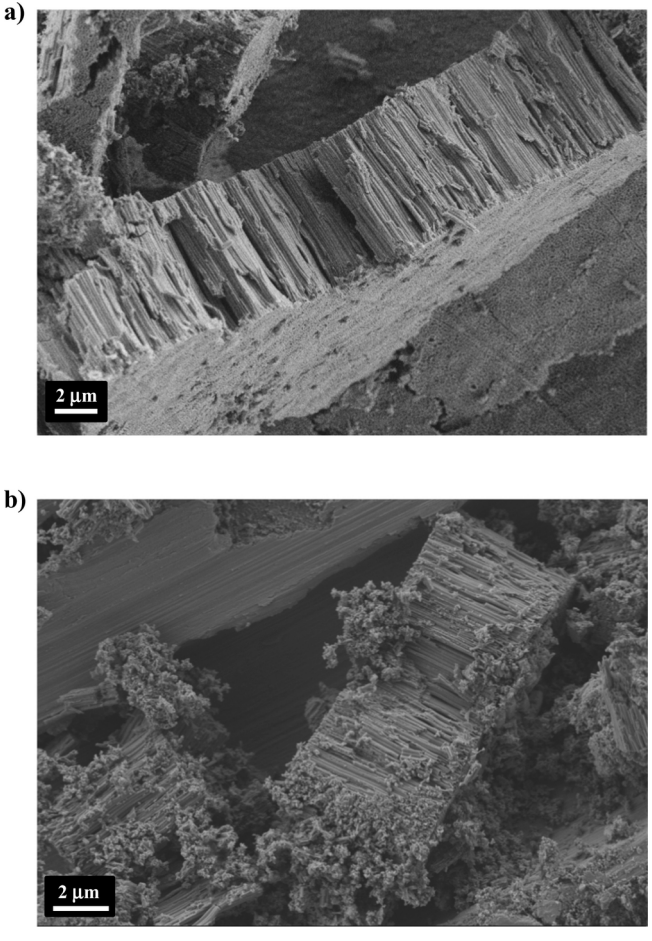

Figure 5

a

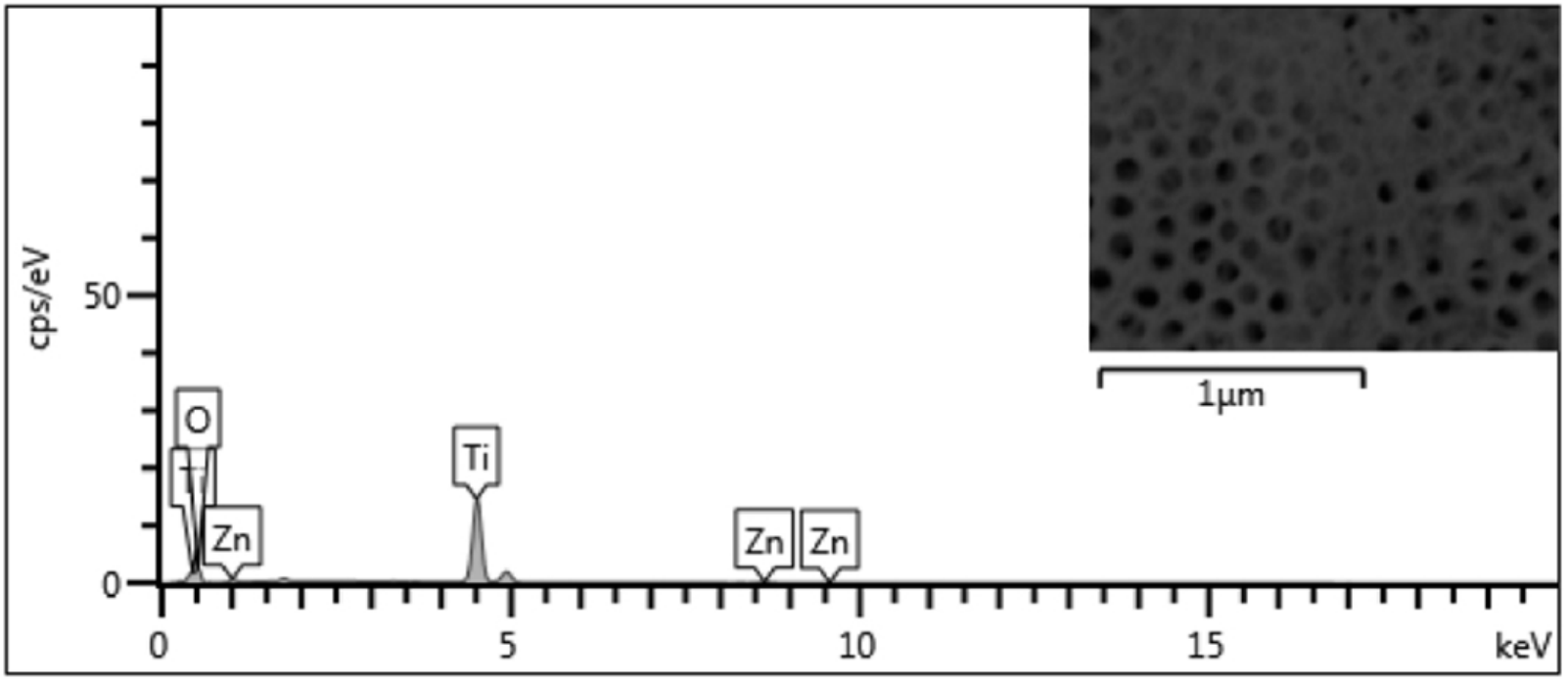
cps/eV
50
0
O
Zn
Ti
Zn
Zn
0
5
10
15
keV
1µm

b

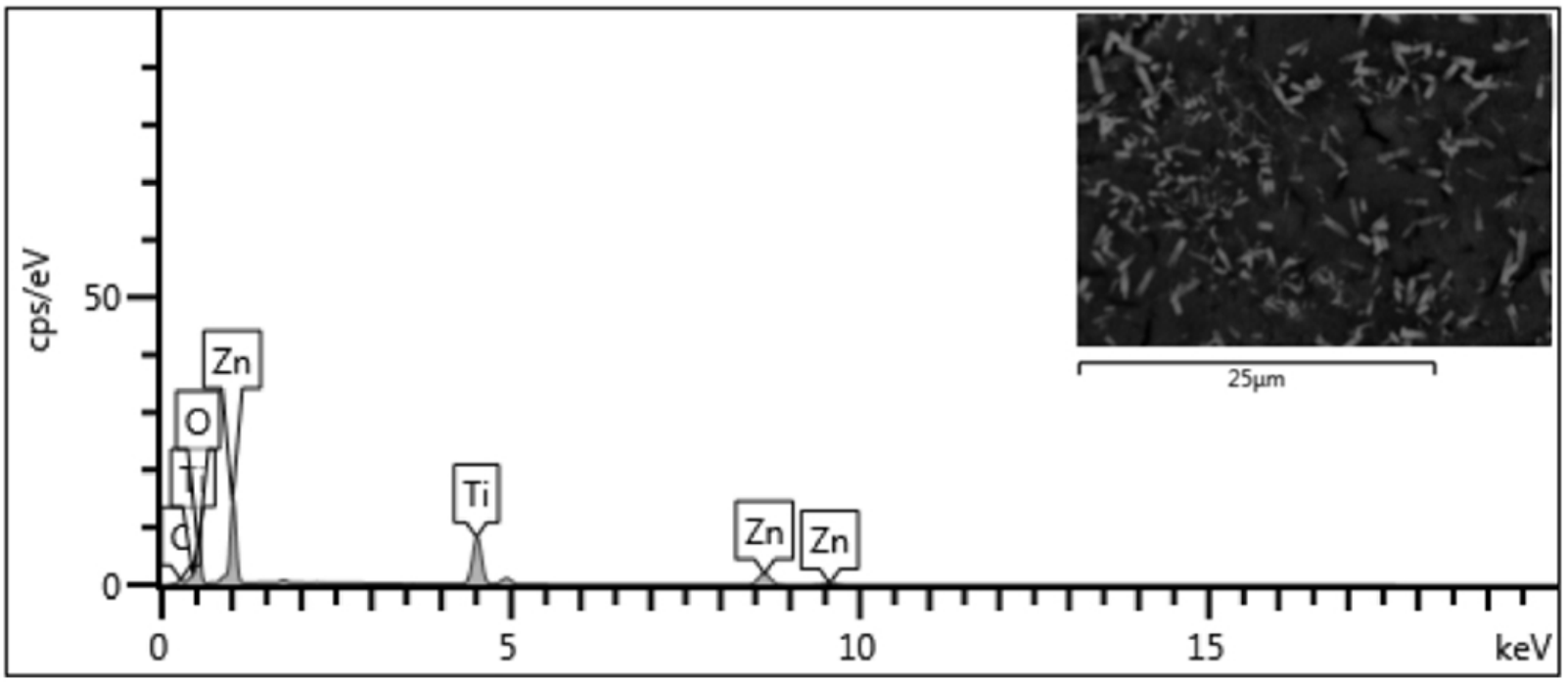
cps/eV
50
0
Zn
O
Ti
Zn
Zn
0
5
10
15
keV
25µm

Figure 6

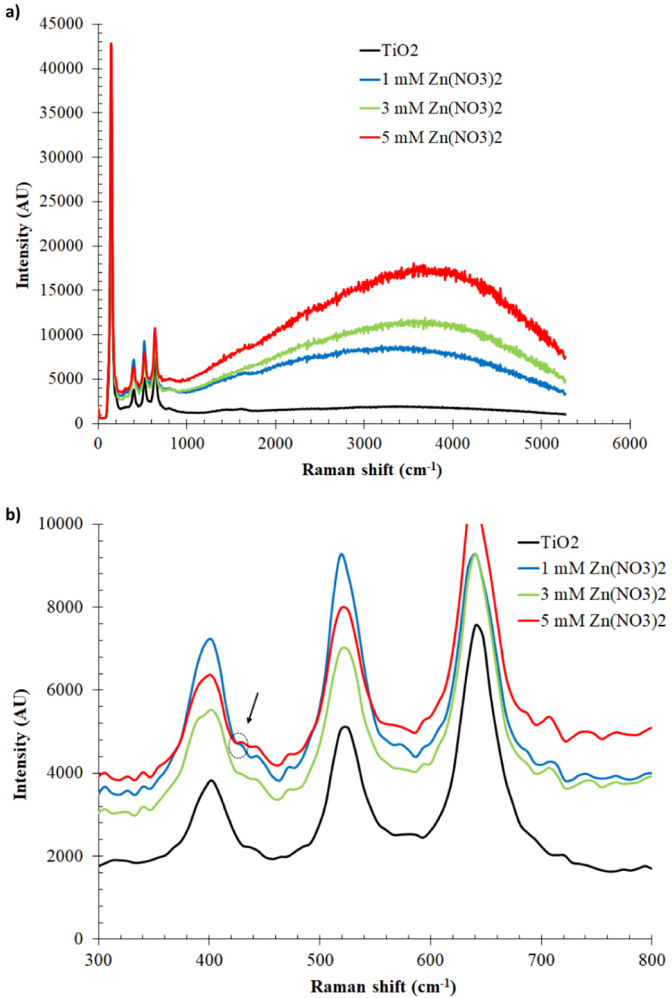
a)
TiO2
1 mM Zn(NO3)2
3 mM Zn(NO3)2
5 mM Zn(NO3)2
Intensity (AU)
Raman shift (cm-1)
b)
TiO2
1 mM Zn(NO3)2
3 mM Zn(NO3)2
5 mM Zn(NO3)2
Intensity (AU)
Raman shift (cm-1)

Figure 7

a) TiO_2

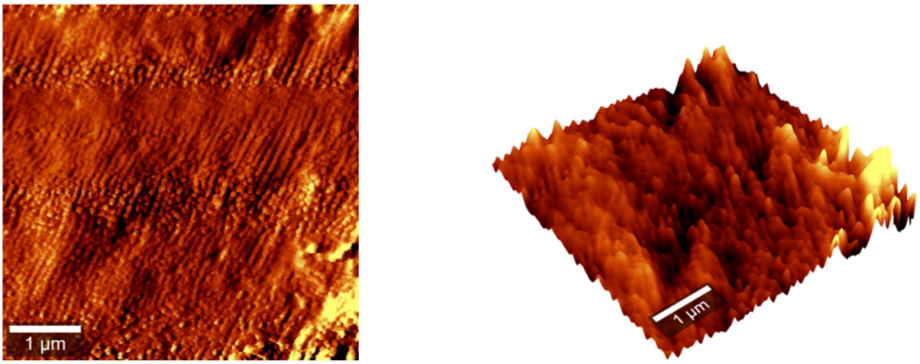

b) $ZnO\text{-}TiO_2$ (5 mM $Zn(NO_3)_2$ – 25 ºC)

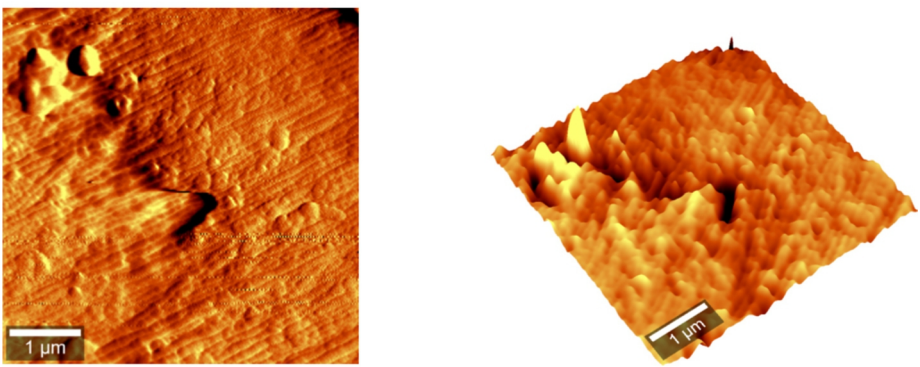

c) $ZnO\text{-}TiO_2$ (5 mM $Zn(NO_3)_2$ – 65 ºC)

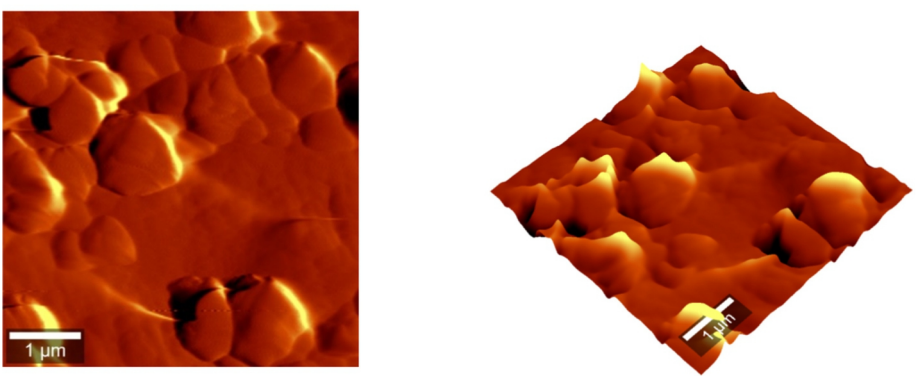

Figure 8

1 mM $Zn(NO_3)_2$

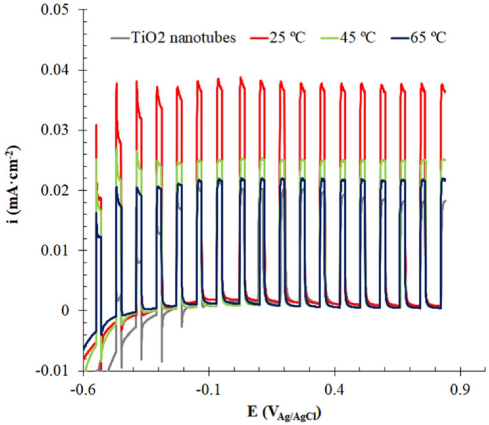

3 mM $Zn(NO_3)_2$

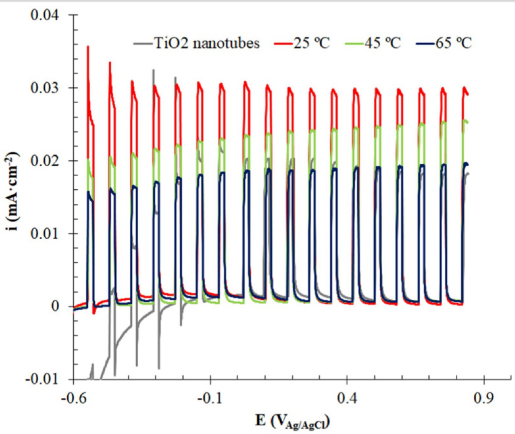

5 mM $Zn(NO_3)_2$

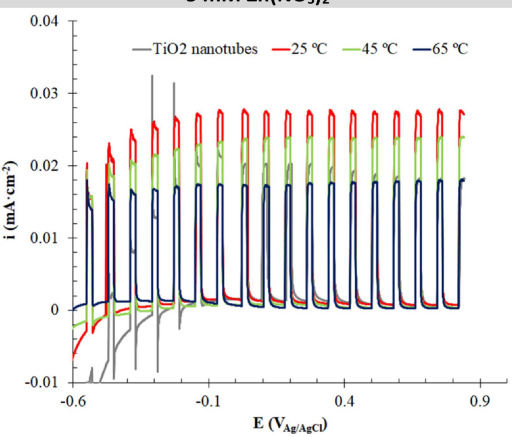

Figure 9

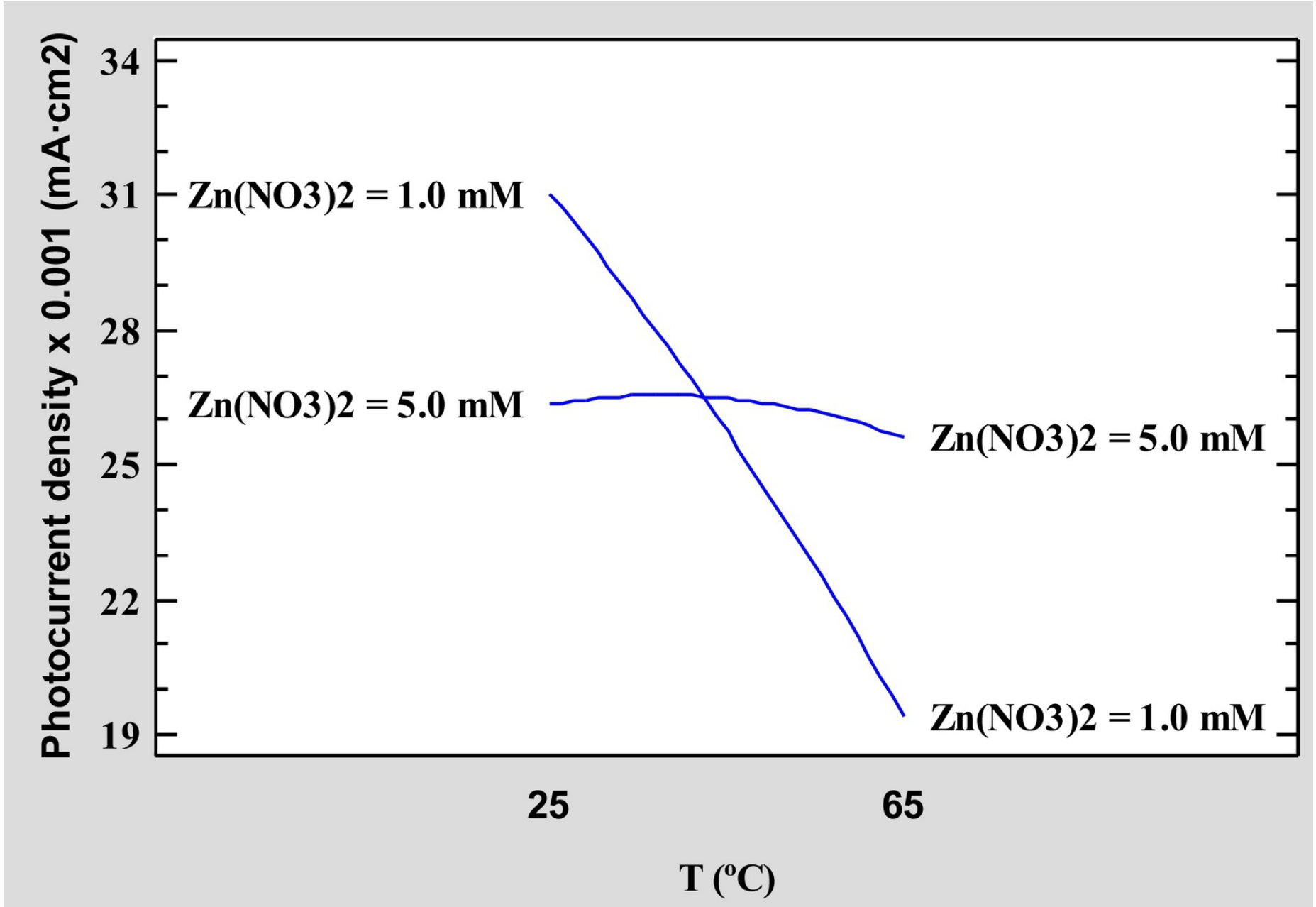
Photocurrent density x 0.001 (mA·cm2)
34
31
28
25
22
19
Zn(NO3)2 = 1.0 mM
Zn(NO3)2 = 5.0 mM
Zn(NO3)2 = 5.0 mM
Zn(NO3)2 = 1.0 mM
25
65
T (ºC)

Figure 10